Precision Engineering 44 (2016) 171–179

Contents lists available at ScienceDirect

Precision Engineering

journal homepage: www.elsevier.com/locate/precision

Optimization of resolution by FDTD analysis in aligner lithography

Seiro Murakami [a,*], Masashi Saito [a], Osamu Yoshida [b]

[a] Optics Center, Cerma Precision, Inc., 16-1, Fuyuki, Koto-ku, Tokyo, Japan
[b] Engineering Department, Japan Science Engineering Co., Ltd. , 1, Kuguso, Terado-cho, Mukou-city, Kyoto, Japan

ARTICLE INFO

Article history:
Received 23 August 2015
Received in revised form
18 November 2015
Accepted 30 November 2015
Available online 23 December 2015

Keywords:
Mask aligner
Fresnel diffraction
FDTD analysis
Pseudo-pattern
Collimation angle
Line width error
Design fidelity
Process change
Multiple smoothing illumination optical system
Adjustable aperture mechanism

ABSTRACT

A mask aligner can transcribe a pattern from a photomask to an exposure substrate by Fresnel diffraction. A diffraction fringe, specific to Fresnel diffraction, appears on a light intensity distribution of the pattern (a diffraction pattern image), and the formation of the pseudo-pattern restricts the resolution performance. The diffraction fringe can be smoothened by expanding the spread of the illumination source, and thus, the pseudo diffraction can be attenuated. However, this also causes a change in light intensity at the pattern edge to be attenuated, and the error of pattern line width to process change becomes large. Since edge diffraction patterns can be calculated by finite difference time domain (FDTD) analysis, the size of light source providing optimum resolution can be predicted by calculating and comparing pattern images corresponding to the size of the light source using this analysis. Therefore, by introducing an illumination optical system that can arbitrarily set the size of a light source to a predicted value, optimum resolution can be obtained without prior trial exposure. This study shows that the resolution of an aligner can be optimized by prior prediction, by introducing a multiple smoothing optical system that has been developed as an illumination system. This system realizes uniform illumination distribution on both a pupil plane and photomask plane and has an adjustable aperture mechanism that, by combining it with FDTD analysis, can arbitrarily set the size of the light source.

1. Introduction

Mask aligners (hereinafter referred to as aligners) have been used for exposing pattern of line widths in the range of a few to several tens of micrometers in a production line [1]. Aligners are used in lithography because of their simplicity and low price, and additional applications, such as achieving high-step exposure in the production of MEMS (micro electro-mechanical systems), have also been reported in recent years [2]. With respect to miniaturization, although in the submicrometer field an imaging method of a projection optical system is superior because of fundamental limit, in the micrometer field, resolution performance improvement has been attempted by aiming to form more stable exposure patterns with less line width error [3].

In general, resolution performance depends on the light intensity distribution of a pattern image formed by an optical system. In lithography, a sharper change in light intensity at a pattern edge leads to lesser change in the pattern line width after development, which is caused by changes in exposure/process conditions, (hereinafter referred to as the process change), and hence the resolution practically achievable is high [4]. An exposure pattern with an aligner is formed by Fresnel diffraction. A characteristic problem in proximity exposure is that it is necessary to control the diffraction light intensity distribution at the edge using an optical system. Since the light intensity distribution of a pattern image in Fresnel diffraction can be calculated by FDTD (finite-difference time-domain) analysis [5,6], a rigorous electromagnetic field analysis method, a diffraction pattern image can be predicted exactly under each condition by presetting the desired pattern shape, illumination conditions, and gap size. Therefore, the size of light source that maximizes a light intensity change at a pattern edge can be predicted in FDTD analysis with a pseudo-pattern image, controlled by changing the size of the light source that is one of the illumination conditions, and comparing the obtained diffraction pattern image. By setting the size of a light source predicted beforehand to an aligner, an optimum resolution can be obtained without trial exposure.

To realize the optimum resolution predicted from FDTD analysis, an illumination optical system that can set any size of light source, based on the prediction in the actual pattern exposure, is needed. However, with a conventional aligner illumination system, a plate corresponding to the desired shape of light source is selected from

* Corresponding author. Tel.: +81 43 294 8342; fax: +81 43 294 8342.
E-mail address: murakami.s@eastcom.ne.jp (S. Murakami).

http://dx.doi.org/10.1016/j.precisioneng.2015.12.002
0141-6359/

plurals prepared beforehand and installed [7–9]. Thus, it is difficult to adjust the equipment to achieve the size of light source predicted by FDTD analysis. As a prerequisite for light sources of any size, a uniform illumination distribution across the whole light source area is required. In conventional optical illumination systems, the uniformity of the final illumination distribution on the photomask plane has been established, but uniformity of the whole light source area is typically inadequate [3].

To optimize the resolution of an aligner, this study describes the following:

(1) a multiple smoothing optical illumination system that achieves a uniform illumination distribution on both the optical pupil plane (corresponding to a light source) and photomask plane,
(2) an adjustable aperture mechanism that can arbitrarily set the size of the light source.

Furthermore, we combine these two features with FDTD analysis and propose a resolution optimization technology that features prior prediction.

2. Optimization of resolution by FDTD analysis

2.1. Pattern image by Fresnel diffraction

2.1.1. FDTD analysis

With an aligner, a diffraction pattern image is formed by Fresnel diffraction with a photomask and an exposure substrate in proximity [1,4,10]. This is shown in Fig. 1. To estimate the resolution performance, the calculation and evaluation of diffraction pattern images are needed; in this article, the above FDTD analysis was introduced as a numerical analysis simulator. The bottom of Fig. 1 shows diffraction pattern images obtained through this analysis.

The FDTD analysis used in this article is discussed below. In general, handling the diffraction phenomena includes using scalar and vector diffraction theories; when micro objects at the wavelength level are handled or when polarization becomes a problem, the latter is used [10]. Because this article discusses the handling of several μm patterns, no need exists to discuss the differences between the handling methods. Vector diffraction was used in consideration of a future evaluation of the resolution limit and versatility of the product design of the aligner manufactured by trial, as discussed in this article. The FDTD and rigorous coupled-wave analysis (RCWA) methods are known as major analysis methods using vector diffraction [11]. When the periodic structure is analyzed, the RCWA method, which is capable of high-speed processing, is used, and when the aperiodic structure is analyzed, the FDTD method is used [12]. This article evaluates the periodic 5 bar-patterns shown in Fig. 1. The versatile FDTD method was used to understand the differences between the central and peripheral patterns of the diffraction images and for the evaluation of isolated patterns in the future. We used the FDTD simulator, FullWAVE, manufactured by SYNOPSYS, which is used widely in the optical field and has a robust performance corresponding to experimental results [13–15]. For boundary conditions of the calculation space in this simulator analysis, we used perfectly matched layer (PML) absorption boundary conditions that were highly precise [16–18]. To avoid the influence on the analytical result, the boundary was separately set several tens of micron meters or more from the photomask pattern and the exposure substrate.

2.1.2. Pattern image changes

Fig. 2 shows changes in diffraction images at the pattern edge when the gap and light source sizes were changed in an aligner. Diffraction light is generated from a pattern edge on an illuminated photomask. For the case of an enlarged gap, the diffraction light expands, the diffraction waveform smoothens, and the diffraction fringe attenuates, as shown at the top and bottom of the figure. On the other hand, with attention paid to the size of a light source, in the case of an expanded light source (i.e., the aggregate of point light sources), the diffraction fringe can be attenuated through a smoothing effect in the same way as an enlarged gap since a diffraction waveform also expands from side to side and overlaps as shown at the top in the figure. Since the size of a light source is nearly in proportion to collimation angle θ (i.e., maximum illumination angle, hereinafter referred to as collimation angle) at the top in Fig. 2, the size of a light source is expressed as collimation angle θ below.

Changes in the line-width pattern are discussed below. In general, the minimum resolution line-width W of a pattern image by Fresnel diffraction is defined with exposure wavelength λ and gap G, and it is expressed as the following equation [4].

$$W \sim \sqrt{G \times \lambda}, \tag{1}$$

as exposure wavelength λ, line i (365 nm), line h (405 nm), and line g (436 nm) are used, which are the bright lines of an ultra-high-pressure mercury lamp (hereinafter referred to as a mercury lamp) that are used generally as an aligner light source. Gap G depends on the warp of a substrate, nonuniformity of a resist film thickness, and

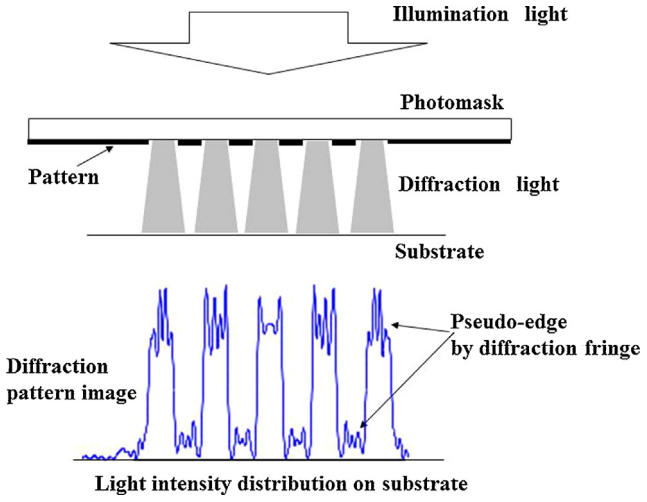

Fig. 1. Fresnel diffraction. The diffraction pattern image is formed by Fresnel diffraction with a photomask and an exposure substrate in proximity.

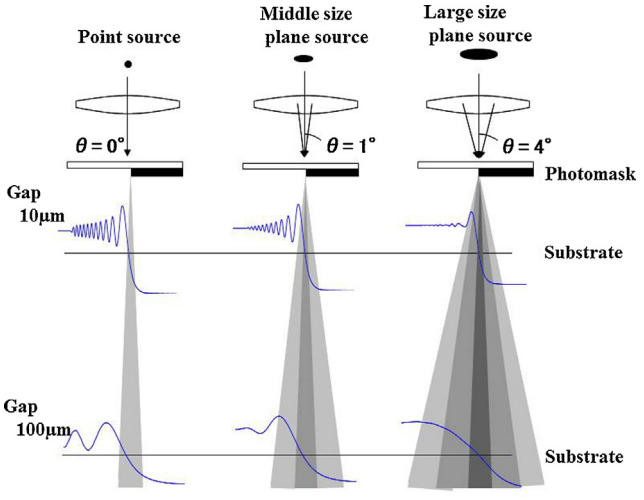

Fig. 2. Changes of diffraction light. The diffraction waveform is smoothed by an enlarged gap and an expanded light source.

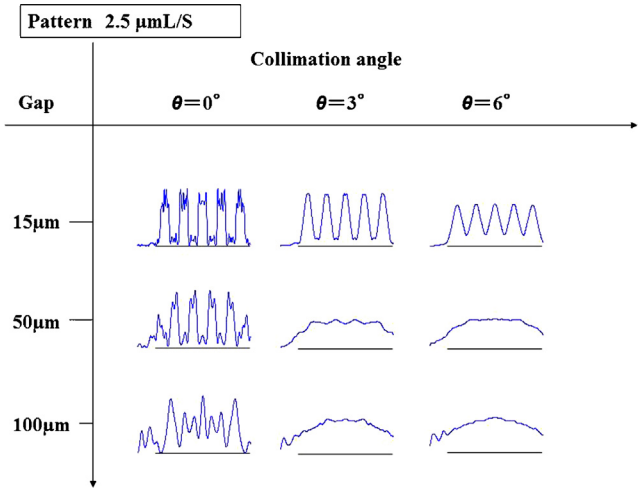

Fig. 3. Diffraction image at 2.5 μm L/S. The collimation angle is changed from 0° to 6° and gap from 15 to 100 μm.

flatness of a substrate holder and is set in a range from several μm to 200 μm [3]. The minimum practical resolution line width depends on the exposure wavelength and gap, and it measures from several μm to 10 μm. Figs. 3 and 4 show diffraction pattern images of 2.5 and 10 μm line and space (L/S) pattern, respectively, when the gap and collimation angle were changed. For the exposure wavelength, line i was used. The figure shows that with the increase in the collimation angle and gap, a pseudo pattern image is attenuated, and the light intensity change of the diffraction pattern image becomes moderate.

2.2. Resolution optimization and predicted exposure

2.2.1. Resolution performance

Resolution in lithography is evaluated via critical resolution, line width error, and design fidelity of the exposure pattern [1,4]. In this study, line width error and design fidelity are evaluated as resolution performance in aligner.

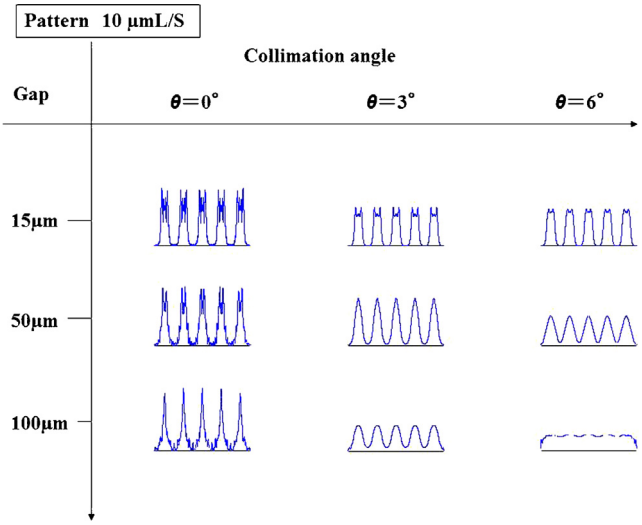

Fig. 4. Diffraction image at 10 μm L/S. The collimation angle is changed from 0° to 6° and gap from 15 to 100 μm.

2.2.2. Definition of resolution performance of diffraction pattern image

The resolution performance of the diffraction pattern image is defined by processing of the diffraction waveform $I(x)$ obtained by FDTD analysis, as shown in Fig. 5. Prior to processing, when a pseudo-pattern image, as shown by the shaded regions at the top and bottom of Fig. 5, exceeds the predetermined level or indicates a low intensity change, it is excluded from evaluation. The line width Lw of a pattern is obtained when the slice level traverses $I(x)$. The slice level is defined by the average intensity of diffraction waveform $I(x)$.

(1) Line width error

The line width of a pattern varies due to the process change. For example, when exposure intensity increases in process, an edge is formed at a lower position in diffraction waveform $I(x)$ of the pattern image after development. That is, the process change is equal to the intensity change of the pattern diffraction image $I(x)$ and the range of the slice level change, shown by the lightly shaded region at the center of Fig. 5, corresponds to the line width error of the pattern after development. Therefore, the sharper the change in intensity of diffraction waveform $I(x)$, the smaller the line width change of a pattern to the process change, and thus, the higher the practical resolution of the lithography. An error window (i.e., the error margin, hereinafter referred to as error window), as shown in Fig. 5, has a vertical length corresponding to the range of the process change and a horizontal length corresponding to the line width error limit. To facilitate comparison under each condition, the range of process change is fixed as ±10%. The sharpness of the intensity change of diffraction waveform $I(x)$ is defined with a differential value at a slice level shown in the following equation as intensity slope I_s.

$$I_s = \frac{dI(x)}{dx}\Big|_{\text{Slice level}}, \tag{2}$$

The application of an intensity slope to the error window determines the line width error.

(2) Design fidelity

In this study, the design fidelity is evaluated via the ratio of the space pattern to pattern pitch, and is called the duty ratio, as follows. Duty ratio Dr is defined by the following equation with the

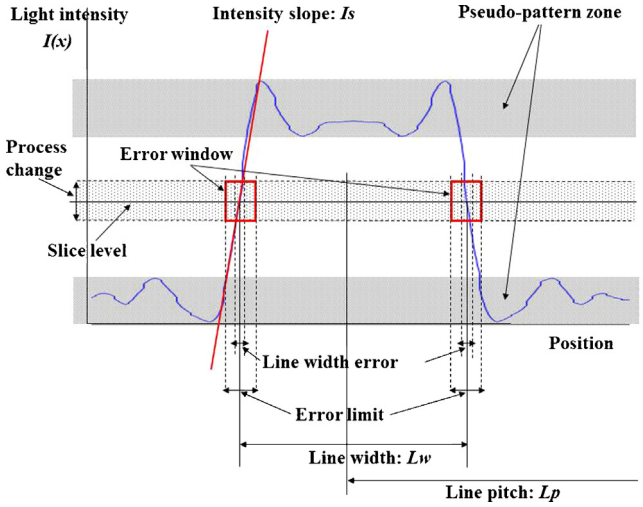

Fig. 5. Resolution in Fresnel diffraction. The application of an intensity slope to the error window determines the line width error. The design fidelity is evaluated via the ratio of the line width to line pitch.

distance between the centers of adjacent patterns used as the line pitch *Lp*.

$$Dr = \frac{Lw}{Lp}, \tag{3}$$

2.2.3. Resolution optimization

A change in the diffraction pattern image, as shown in Figs. 3 and 4, exhibits that an optimal size and a gap of the light source exist that attenuate a pseudo-pattern image to the predetermined range and maximize the light intensity change near the slice level.

(1) Determination of control method

The advantages of the aligner exposure include its high productivity, which is capable of batch exposure in an area of several inches; this condition requires the achievement of a uniform resolution performance across an exposure surface. The distance between the photomask plane and the substrate plane is locally non-uniform because of the warpage of the exposure surface, owing to, for example, the thickness non-uniformity of the resist film, warpage of the substrate, or flatness of the substrate holder. It is, therefore, difficult to ensure a uniform resolution performance across the whole exposure surface using gap control. When the size of the light source is controlled, the illumination uniformity on an exposure surface is also required. With our newly developed illumination optical system, the resolution was optimized by controlling the size of the light source and ensuring the illumination uniformity across the exposure surface.

(2) Optimum resolution and predicted exposure

In this study, the size of the light source that provides both a line width error and duty ratio within their error limits is defined as the collimation angle that provides the optimum resolution. Realization of optimum resolution performance is verified by predicting, prior to exposure, a collimation angle that provides an optimum resolution and thereby making the size of a light source exposure correspond to the predicted value.

3. Experimental method

3.1. Prototype aligner

Fig. 6 shows the configuration of a prototype aligner developed for optimum resolution predicted exposure. After passing through an illumination optical system consisting of the first and second lens groups, the illumination from a mercury lamp (Hg lamp) illuminates a photomask plane. An adjustable aperture is attached between the first and second lens group to define the size of the light source. After an exposure substrate is transferred and mounted on the substrate holder under a photomask, the substrate stage is moved in the *Z*-axis direction and positioned at the predetermined gap by the gap sensor. After the pattern information (including the L/S design values) for the photomask have been inputted in the computer, a diffraction pattern image corresponding to the pattern information and set gap amount is calculated by the FDTD simulator (which is incorporated in the computer). A pattern image is calculated for each collimation angle, and the determination of a pseudo-pattern and calculation of the line width error and duty ratio is carried out, as described in Section 2.2, for each pattern image. Following this, a collimation angle that predicts the optimum resolution is determined. Then, a light source image corresponding to the prescribed size is set by the adjustable aperture mechanism according to the predicted value and exposure takes place.

Table 1 shows the main specifications of the prototype aligner. The exposure wavelength is i-line (i.e., 365 nm), and the exposure area is 100 mm^2, to ensure practical use as a batch aligner.

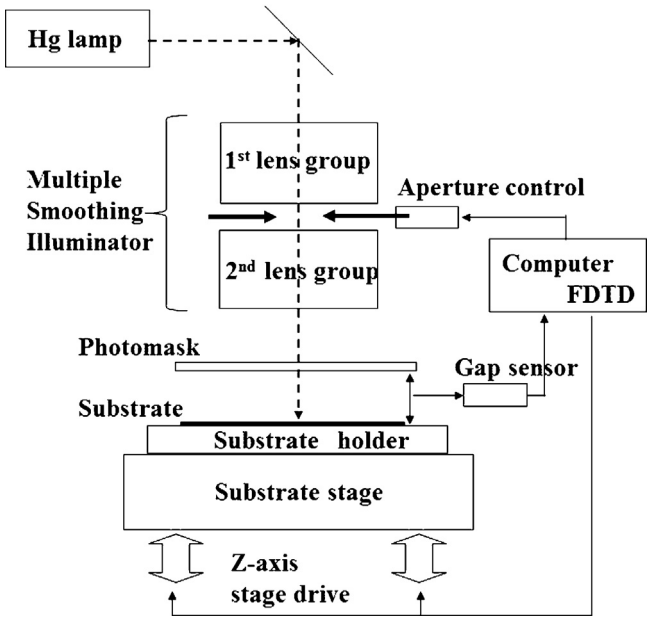

Fig. 6. Prototype exposure system. The configuration consists of a Hg lamp, an illuminator, an aperture control, a photomask stage, a substrate stage, and a computer with FDTD.

3.2. Multiple smoothing illumination optical system

There are two prerequisites for an illumination optical system to optimize resolution by predicted exposure, which are as follows:

(1) uniformity of illumination intensity on a photomask plane
(2) uniformity of brightness across the whole light source area (light source surface).

A conventional aligner illumination system meets the requirement of the uniformity of illumination intensity on a photomask plane, Task (1). However, in this conventional setup, the light source illuminating the photomask is only a projection of a light-emitting point of a mercury lamp, and it is difficult to form an expanded light source image and then make its size variable (Task (2)) [3].

Fig. 7 shows the configuration of the newly developed illumination optical system that does address these issues. The first and second lens groups are arranged to the left and the right of the pupil plane, acting as the center, respectively. The first lens group forms a light source image (secondary light source), and the second lens group illuminates the photomask plane. Light emitted from a light-emitting point of a mercury lamp, which is placed at the first focal point of an elliptic mirror, is collected at the second focal point and then enters the first lens group. The non-uniformity of illumination in an aligner illumination optical system is mainly due to the brightness distribution of the mercury lamp; there is non-uniformity in

Table 1
Specifications of prototype exposure system.

Exposure wavelength		i-Line 365 nm
Exposure field		100 mm × 100 mm
Illumination optics	Power (on photomask)	300 mW/cm^2
	Uniformity 1 (on photomask)	±2%
	Uniformity 2 (on puple plane)	±2%
	Collimation angle (on photomask)	Range 1–6° Minimum setting 0.1°
Substrate stage	Gap setting	Range 10 μm–1 mm Minimum setting 1 μm

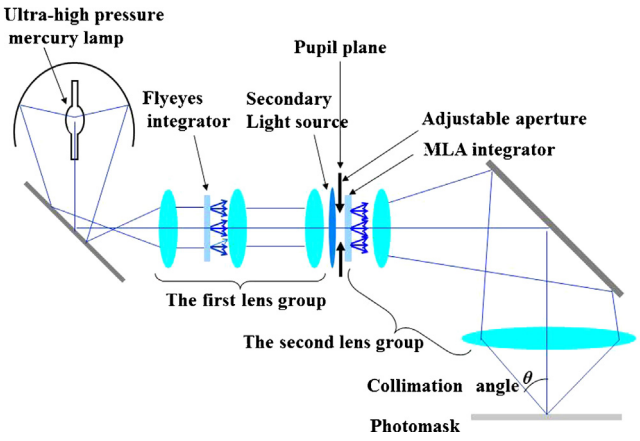

Fig. 7. Multiple smoothing illumination optical system. Optical system is composed of the first lens group with Flyeyes and second lens group with MLA.

the plane and in the irradiation direction because of the irradiation angle distribution. In the first lens group, a fly-eye optical system is used as an optical integrator to convert non-uniformity in the irradiation direction to non-uniformity in the plane. Each point in the plane illuminates the whole pupil plane via the subsequent lenses, and the whole pupil plane is uniformed. This ensures the uniformity of illumination intensity on the optical pupil plane where the secondary light source image is formed [1,3,4,10,19]. In the second lens group, a micro lens array (MLA) is used as an optical integrator to ensure the uniformity of illumination intensity on a photomask plane, in the same way as the first lens group. In this article, a smoothing illumination optical system using a combination of these two lens groups is called a multiple smoothing illumination optical system. This illumination optical system achieved a uniformity of illumination intensity of ±2% or lower on both the pupil and photomask planes, as shown in Table 1.

The specification of an optical integrator, i.e., the main component in this illumination system, is reported below. In general, the smaller the size of an element lens of an optical integrator, such as a flyeye optical system and an MLA, the better the smoothing performance; however, limits exist owing to manufacturing and restrictions based on costs. The diameter of the flyeye element lens used for a standard illumination optical section is approximately 4–10 mm and that of an MLA is approximately 300–500 μm [20]. The cost of an MLA is higher than that of a flyeye optical system by approximately one order. As described above, the optical integrator, which is used as the first lens group of this illumination system, was a flyeye optical system, and the specified value of the diameter of the element lens was 5 mm. This specification corresponds to a desired value in the optical design necessary to ensure a uniformity of illumination intensity of ±2% on the pupil plane, as shown in Table 1. As described above, the optical integrator used as the second lens group was an MLA, not a flyeye optical system, and the specified value of the diameter of the element lens was 300 μm. The size of the light source image on the pupil plane that enters the second lens group can be changed arbitrarily with the adjustable aperture, as shown in Fig. 7. When a small collimation angle is set, the light source image is also narrowed. When a normal flyeye optical system is used as the second lens group, the minimum element size is approximately 4 mm, as described above, and a sufficiently small element size is not obtained for a narrowed light source size. The number of secondary light sources divided by the element, therefore, decreases, and the uniformity of the illumination intensity on the photomask plane cannot be maintained. The MLA, i.e., the element size that is one tenth or lesser the size of the flyeye optical system, was used to ensure the uniformity of the illumination intensity on the photomask plane. The abovementioned value of 300 μm of the MLA element lens diameter corresponds to the desired value in optical design necessary to ensure a uniformity of illumination intensity of ±2% on the photomask plane in the variable range of collimation angles, as shown in Table 1.

3.3. Evaluation of exposure pattern

The relationship between the resolution performance predicted by FDTD analysis, described in Section 2.2 and obtained by an exposure pattern with a prototype aligner, described in Section 3.1, was studied. Fig. 8 shows a pattern diagram indicating a diffraction pattern image after photomask permeation and a pattern after exposure/development. The resist was positive. The intensity distribution $I(x)$ of the diffraction pattern image is shown at the top of the figure, and the latent image distribution in the resist exposed according to $I(x)$ is shown in the middle. Shading in the figure indicates the degree of energy absorption after the exposure time had elapsed; the energy absorption was larger inside the resist. The dotted line shows the energy threshold at which the resist dissolves at development [21], and the cross-section shape $H(x)$ of the resist pattern after development, which was determined by the energy threshold, is shown at the bottom in the figure. Fig. 9 shows a pattern diagram indicating the observation of a pattern after development from above with an optical microscope. The observed image signal $R(x)$ shown at the bottom of the figure corresponds to the intensity distribution of reflected light taken in a solid angle specified by the numerical aperture (NA) of the microscope. In a device that comprises a silicon substrate and photo resist, which are commonly used for semiconductor lithography, reflected light from substrate (c), the base, is strongest, and reflected light from the right and left resist pattern surfaces (a) is next strongest, as shown in figure. On the other hand, at pattern edge (b), the reflected light and scattered light taken in the NA of the microscope is lower and

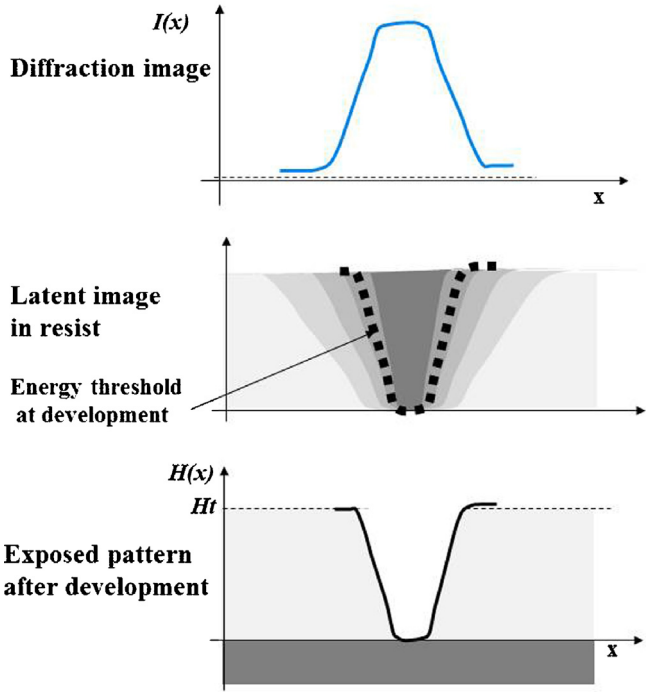

Fig. 8. Relation between the diffraction image and the exposed pattern. Top, middle, and bottom sections of the figure show the diffraction pattern image, the latent image distribution in the resist, and the cross-sectional shape of the resist pattern after development, respectively.

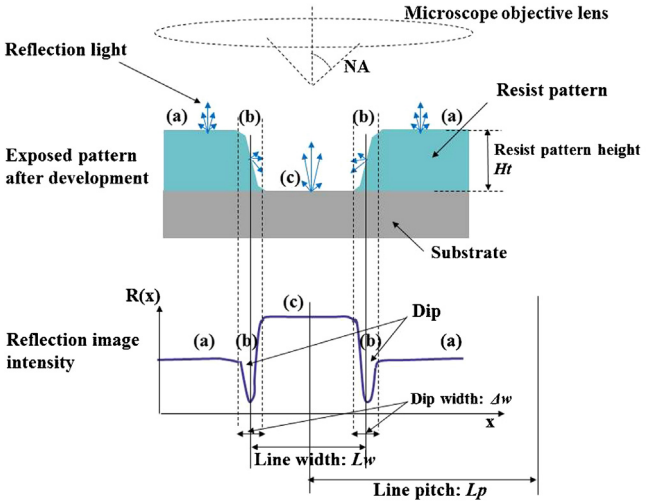

Fig. 9. Definition of resolution in exposed pattern. Top, middle, and bottom sections of the figure show the optical microscope to observe the exposed pattern, cross section of the resist pattern, and observed image signal to determine resolution performance, respectively.

intensity is weak. A dip in intensity, therefore, appears at a place corresponding to the pattern edge in reflected light intensity distribution $R(x)$ [22], and dip width Δw corresponds to the edge area width of the exposure pattern. The line width Lw of the exposure pattern is calculated and defined as the distance between the right and left dip centers. The resolution performance of an exposure pattern based on waveform processing of $R(x)$ is defined below.

(1) Line width error

As described above, dip width Δw in an observed image $R(x)$ corresponds to the edge area width of an exposure pattern; the larger the dip width, the shallower the slope of cross-section of the edge. In this study, the edge slope Es is defined below as the edge slope of an exposure pattern [23].

$$Es = \frac{Ht}{\Delta w}, \tag{4}$$

where Ht is the height of a resist area in a cross-sectional pattern $H(x)$, as shown in Figs. 8 and 9, and corresponds to the thickness of a resist film. As shown in the process of the exposure pattern formation in Fig. 8, the sharper the intensity slope of the diffraction pattern image, generally the narrower is the edge area of an exposure pattern and the relatively sharper is an edge slope, as shown in Eq. (4) [4]. The relationship between the edge slope and the line width error is discussed below. The exposure energy distribution $E(x)$ of a resist is expressed as the following equation, with the exposure time expressed by T.

$$E(x) = I(x) \times T, \tag{5}$$

$E(x)$ is converted to a latent image distribution by the exposure absorption process in the resist and changes to the final cross-section shape profile $H(x)$ occurs through the development process. By increasing exposure dose E to a resist of predetermined film thickness Ht, and determining the maximum exposure dose E_{max} at which the base substrate appears after development, the height Ht of a cross-section pattern (corresponding to the resist film thickness) can be made to correspond to the maximum intensity of pattern image I_{max} (corresponding to E_{max}/T). With respect to the process change, therefore, an intensity change of pattern image I_{max} can be treated as a change of film thickness Ht of the exposure pattern. By applying the edge slope shown in Eq. (4) as a change of Ht to the vertical axis in an error window is defined in Section 2.2.2, a line width error of an exposure pattern can therefore be evaluated.

(2) Duty ratio

The line width Lw and line pitch Lp shown at the bottom of Fig. 9 are used to define the duty ratio by Eq. (3), in the same way as for a diffraction pattern image.

Based on the above definition of an exposure pattern shape, optimum resolution predicted exposure, achieved by control of the light source size, can be verified by experiment.

4. Experimental results

The results of exposure with the prototype aligner are reported here. The minimum practical resolution line width of the aligner

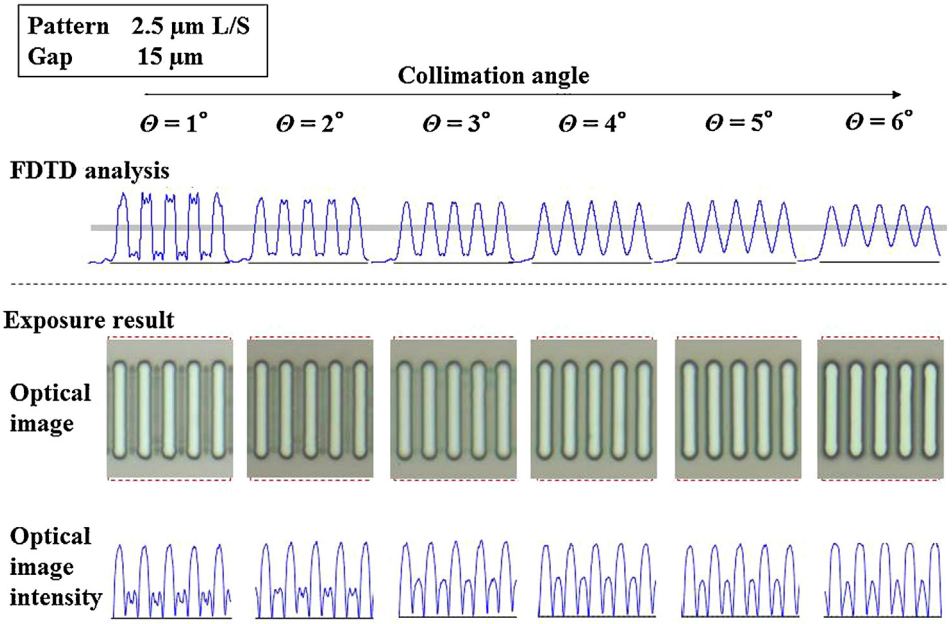

Fig. 10. FDTD analysis & experimental result in 2.5 μm L/S. Corresponding to the collimation angle changed from 1° to 6°, the diffraction pattern image obtained by FDTD analysis is shown at the top section, the optical microscope image of a pattern after development at the middle section, and the observed image signal at the bottom section of the figure, respectively.

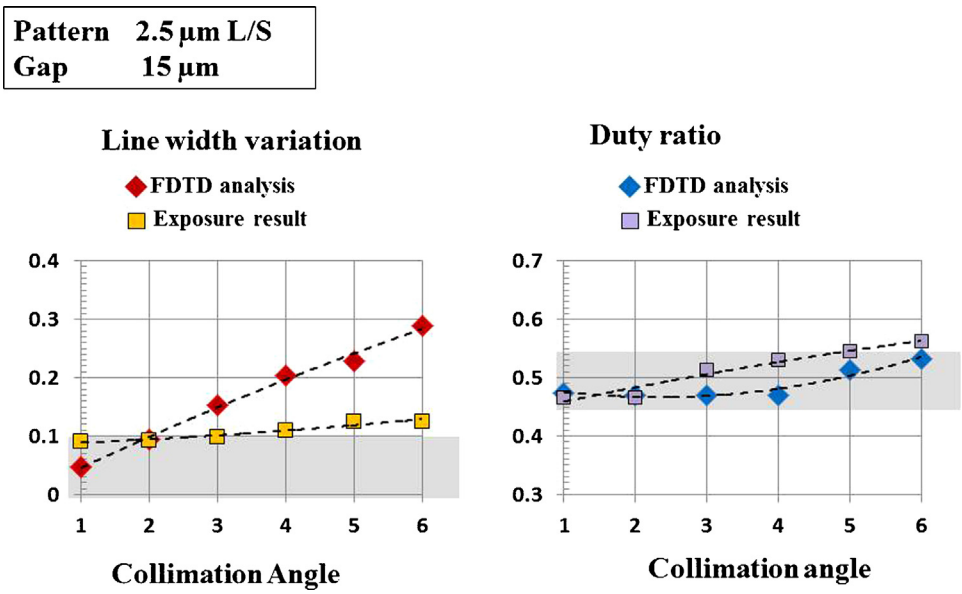

Fig. 11. Comparison between the FDTD analysis & the exposure result in 2.5 μm L/S. Corresponding to the change of the collimation angle from 1° to 6°, the resolution performance as predicted by an FDTD analysis and as obtained from the exposure results are shown. The figure on the left provides the details of the line width error, and the figure on the right provides the details of the duty ratio.

depends on the exposure wavelength and gap, as explained in Section 2.1.2, and changes from several μm to 10 μm. In our study, line i was used as the exposure wavelength, and the following were used as evaluation patterns.

(a) 2.5 μm L/S pattern, 15 μm gap.
(b) 10 μm L/S pattern, 100 μm gap.

Figs. 10 and 12 show a diffraction pattern image $I(x)$ (top) by a FDTD analysis with a change of the collimation angle from 1° to 6°, a pattern image with an optical microscope (middle) after development and an image signal $R(x)$ (bottom) at 2.5 and 10 μm L/S, respectively, were formed. Table 2 shows the experimental conditions.

Figs. 11 and 13 show the values predicted by a FDTD analysis and exposure results concerning resolution performance with a change of the collimation angle. The dotted line in the figure corresponds to the approximated curve for each data point. The left figure gives the details of the line width error and shows the + side error in percentage. The right figure gives the details of the duty ratio: the duty error is 0 at a duty ratio of 0.5. The gray area in the figure corresponds to a tolerance of ±10%, which is a common design rule [1]. Because the collimation angles of 4–6° for the 10 μm L/S did not meet wave shape processing criteria, they were excluded from the evaluation.

The analysis-predicted values and exposure results of the collimation angles that provided resolution performance thereby satisfying a tolerance of 10% are compared below.

(a) 2.5 μm L/S pattern, 15 μm gap
- Line width error: Although both have the same tendency of errors, as the collimation angle increases, the change in the exposure results is moderate.
- Predicted value: 1–2.1°, exposure result: 1–3.1°
- Pattern duty: Both show a similar tendency.
- Predicted value: 1–6°, exposure result: 1–4.7°
- Optimum resolution: Predicted value: 1–2.1°, exposure result: 1–3.1°.

(b) 10 μm L/S pattern, 100 μm gap
- Line width error: Although both exhibit the minimum values, when the collimation angle is near 2.3°, the change of exposure results is moderate.
- Predicted value: 2–2.5°, exposure result: 1–3°
- Pattern duty: Although both show a similar tendency, the change in exposure results is moderate.
- Predicted value: 2.2–3°, exposure result: 1.2–3°
- Optimum resolution: Predicted value: 2.2–2.5°, exposure result: 1.2–3°.

Table 2
Experimental condition.

Wavelength	i-Line 0.365 μm	
Substrate	Silicon wafer	
Resist	MCPR is 101 K (Rohm and Haas) Thickness 1 μm positive-resist	
Exposure dose	50 mJ/cm^2	
Development	• Developer	MF CD-26 (Rohm and Haas)
	• Developer volume	200 cm^3
	• Method	Dipping
	• Development time	90 s
	• Rinse	Pure water
	• Rinse time	30 s
Observation	• Instrument	Optical microscope
	• Objective magnification/NA	50/0.8 (at 2.5-μm L/S) 20/0.45 (at 10-μm L/S)
	• Illumination	Bright-field Epi-illumination

5. Considerations

The difference between the FDTD analysis and the experimental results is discussed below. As explained in Section 4, the experimental results show a similar tendency in the change of resolution performance with the collimation angle, which shows that the size of the light source providing optimum resolution can be predicted within a prescribed range. A difference exists between them; however, the changes in line width error and absolute value of pattern duty and exposure results show a moderate change.

This difference is described below. The following primary change and error factors in the diffraction pattern image $I(x)$ to

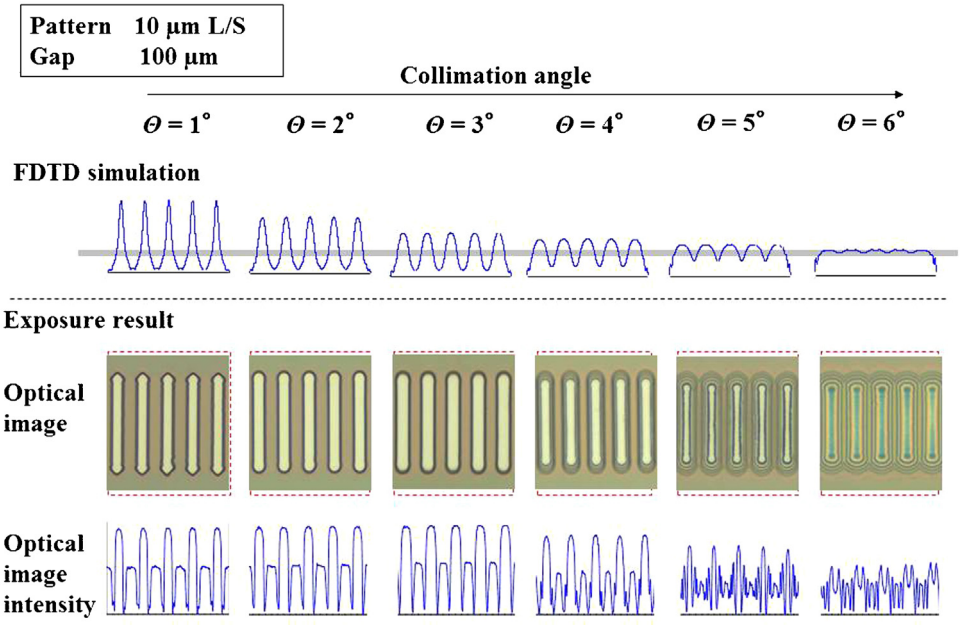

Fig. 12. FDTD analysis & experimental result in 10 μm L/S. Corresponding to the change of the collimation angle from 1° to 6°, the diffraction pattern image obtained by FDTD analysis is shown at the top section, the optical microscope image of a pattern after development at the middle section, and the observed image signal at the bottom section of the figure, respectively.

the reflected light intensity profile $R(x)$ of an exposure pattern are considered:

(1) the illumination optical system: uniformity of brightness of light source image, uniformity of illumination intensity in photomask plane;
(2) the photomask: drawing dimension error of L/S pattern;
(3) the gap: non-uniformity of resist film thickness, warpage of substrate, flatness of substrate holder;
(4) the exposure process: conversion to latent image distribution in resist by exposure, conversion from latent image distribution to cross-section profile by development;
(5) the measuring system: resolution limit and aberration of an optical microscope/image observation system
(6) the processing system: a difference in the waveform processing algorithm between the diffraction pattern image $I(x)$ and the exposure pattern image $R(x)$.

Since this research does not cover the uniformity of resolution performance in the exposure surface, the uniformity of illumination intensity in the photomask plane (1) and the flatness in the exposure surface (3) are excluded. The uniformity of brightness of the light source image (1) is ±2% or less, in a light source surface, as shown in Table 1, and its effect on the setting performance of

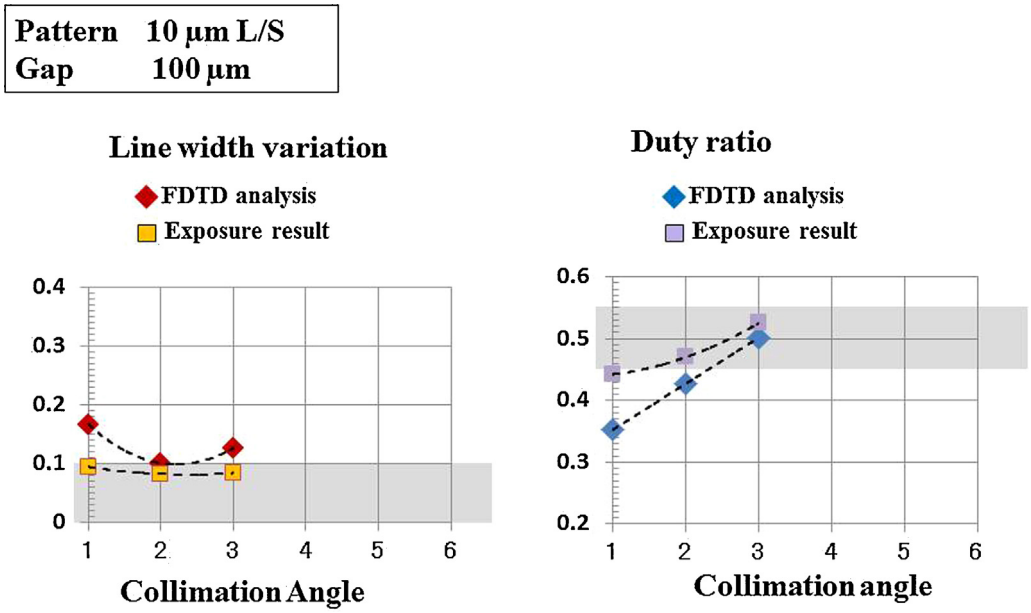

Fig. 13. Comparison between the FDTD analysis & the exposure result in 10 μm L/S.
Corresponding to the change of the collimation angle from 1° to 6°, the resolution performance as predicted by FDTD analysis and as obtained from the exposure results are shown. The figure on the left provides the details of the line width error, and the figure on the right provides the details of the duty ratio.

the collimation angle is small. (2) is 0.1 μm or less, in normal photomask production, and its effect on the pattern sizes of several μm, covered in this study, is small.

The relationship between (4) and the line width error is now considered. In determining the pattern shape after development, an effect of the characteristic curve of photo-resist is large [1,4,21]. This curve indicates the relationship between the exposure energy and the remaining resist film thickness after development; when exposure energy exceeds a certain value, the remaining film thickness generally tends to decrease rapidly. Although the energy distribution of a latent image has an expanded space distribution, it is binarized within a narrow range on the remaining resist film, and the expansion of the slope at an edge is suppressed. As shown on the left of Figs. 11 and 13, therefore, an edge slope change to a collimation angle is relatively smaller than an intensity slope change by the FDTD analysis.

The relationship between (4) and the duty ratio is now considered. Through the FDTD analysis, the size of line width depends on a slice level, as shown in Fig. 5, and the solution energy threshold at image development in the exposure pattern, as shown in Fig. 8. Therefore, criteria for both line widths are different and may become a difference factor of duty ratio shown in the right in Figs. 11 and 13.

Although the resolution of a microscope/image observation system in (5) is approximately 0.3 μm (corresponding to NA 0.8), as shown in Table 2, and although it smooths the reflected light intensity distribution $R(x)$, its effect on resolution at a dip is small, as shown in Figs. 10 and 12.

As for (6), a sharp-edge area with less distortion and change of waveform is used in both $I(x)$ and $R(x)$ as a slice level that determines line width, and error factors are considered to b e less.

6. Conclusion

For resolution optimization of an aligner, the following was achieved:

(1) a multiple smoothing illumination optical system that realizes uniform illumination intensity of ±2% or less, on both an optical pupil plane and a photomask plane was developed,
(2) an adjustable aperture mechanism that can arbitrarily set a collimation angle from 1° to 6° was developed,
(3) a waveform-processing algorithm that quantifies resolution performance of a diffraction pattern image by FDTD analysis and an exposure pattern image with an optical microscope were developed, and
(4) via a combination of the above – (1), (2), and (3) – a collimation angle that provides optimum resolution was predicted by FDTD analysis, and a prototype aligner that can expose at a collimation angle corresponding to the predicted value was developed.

This prototype aligner was used to compare the analysis-predicted values and exposure results of the collimation angles that provided optimum resolution, thereby satisfying a tolerance of 10%, and the following results were obtained.

(a) 2.5 μm L/S pattern, 15 μm gap
Optimum resolution: Predicted value: 1–2.1°, exposure result: 1–3.1°
(b) 10 μm L/S pattern, 100 μm gap

Optimum resolution: Predicted value: 2.2–2.5°, exposure result: 1.2–3°

The exposure results that provided optimum resolution within the predicted values were obtained.

The above discussion showed that the exposure predicted by combining the FDTD analysis in an aligner with a multiple smoothing illumination system is a technology that is useful for resolution optimization under the prescribed exposure conditions.

Acknowledgments

Throughout the preparation of this article, guidance was provided by Professor Hatsuzawa of Tokyo Institute of Technology. Advice was given on optical systems by Professor Shibuya of Tokyo Polytechnic University, and on lithography technology by Professor Tabata and Associate Professor Hirai of Kyoto University. With respect to conducting experiments, assistance was given by Mr. Yamazaki and Mrs. Kaneko of Cerma Precision, Inc. We express our deep gratitude to them all.

References

[1] Lin B. Optical lithography. Bellingham, Washington, USA: SPIE Press; 2009. p. 7.
[2] Yang H, Chao CK, Lin TH, Lin CP. Fabrication of micro lens array with graduated sags using UV proximity printing method. Microsyst Technol 2005; 12(1):82.
[3] Voelkel R. Advanced mask aligner lithography: new illumination system. Opt Exp 2010;18:20972.
[4] Mack CA. Fundamental principles of optical lithography. West Sussex, England: John Wiley & Sons Ltd; 2007. p. 370.
[5] Yee KS. Numerical solution of initial boundary value problems involving Maxwell's equations in isotropic media. IEEE Trans Antennas Propag 1966;14(4):207–302.
[6] Tavlove S. The finite-difference time-domain method. Norwood, MA: Artech House; 1995.
[7] Hornung M, Vogler U, Voelkek R. Customaized illumination for process window optimization and yield improvement in mask aligner lithography systems. J Vac Sci Technol B 2010;28:C6Q6.
[8] Motzek K, Vogler U, Hennemeyer M, Hornung M, Voelkel R, Erdmann A, et al. Computational algorithms for optimizing mask layouts in proximity printing. Microelectron Eng 2011;88:2066.
[9] Motzek K, Partel S, Bramati A, Hofmann U, Unal N, Hennemeyer M, et al. Mask aligner lithography simulation—from lithography simulation to process validation. Microelectron Eng 2012;98:121–4.
[10] Born M, Wolf E. Principle of optics. 7th ed. Cambridge: Cambridge University Press; 1999.
[11] Moharam MG, Gaylord TK. J Opt Soc Am 1982;72–10:1385–92.
[12] Ichikawa H. OSJ 2006;35:340–7.
[13] Ueba Y, Takahara J. Spectral control of thermal radiation by metasurface with split-ring resonator. Appl Phys Express 2012;5:122001–2.
[14] Moriyama Takumi, Tanaka Daiki, Jain Paridhi, Kawashima Hitoshi, Kuwahara Masashi, Wang Xiaomin, et al. Ultra-compact, self-holding asymmetric Mach–Zehnder interferometer switch using Ge2Sb2Te5 phase-change material. IEICE Electron Express 2014;11(15):20140538.
[15] NEDO. Hetero-functional Integrated Device Technology Development Project. In: Final report; 2009.
[16] Railton CJ, Daniel EM. A comparison of the properties of radiating boundary conditions in the FDTD method for finite discretisation and non-planar waves. IEEE Trans Antennas Propag 1994;AP-42(2):276–81.
[17] Andrew WV, Balanis CA, Tirkas PA. A Comparison of the Berenger perfectly matched layer and the Lindman higher-order ABC's for the FDTD method. IEEE Microwave Guided Wave Lett 1995;5(6):192–4.
[18] Berenger J-P. A perfectly matched layer for the absorption of electromagnetic waves. J Comput Phys 1994;114(1):185–200.
[19] Dross O, Mohedano R, Hernandez M, Cvetkovic A, Minano JC, Benitez P. KÖhler integrators embedded into illumination optics add functionality. Proc SPIE Illumination Opt 2008;7103:71030G-4.
[20] Edmund Optics. Optical components catalogue. Barrington, NJ, USA: Edmund Optics Inc; 2015.
[21] Sasaki M. Basics of resist process. IEEJ Trans Sens Micromach 2011;131(1):4.
[22] Reynolds J, Ryde M, Kim H. New advances in reticle qualification techniques. SPIE Opt/Laser Microlith 1988;922:41.
[23] JEITA. Japan Electronics and Information Technology Industries Association: DFM Glossary. JEITA; 2011. p. 39.